Modeling of 3-D Surface Roughness Effects With Application to μ-Coaxial Lines

Milan V. Lukić, *Student Member, IEEE*, and Dejan S. Filipovic, *Member, IEEE*

***Abstract*—Effects of 3-D surface roughness on the propagation constant of transverse electromagnetic transmission lines are calculated using finite-element method software by solving for the fields inside conductors. The modeling is validated by comparison with available literature results for the special case of 2-D surface roughness and by simulations using the finite-integration technique. Results for cubical, semiellipsoidal, and pyramidal indentations, as well as rectangular, semicircular, and triangular grooves in conductor surfaces are presented. A developed surface roughness model is applied to rectangular μ-coaxial lines. It is shown that roughness contributes up to 9.2% to their overall loss for frequencies below 40 GHz.**

***Index Terms*—Attenuation constant, conductor losses, finite-element method (FEM), surface roughness, transmission lines.**

I. Introduction

THE scattering of electromagnetic waves from rough surfaces is a research subject studied by numerous authors for over a century. A comprehensive review of the relevant research literature is available in [1]. The analysis of the interaction between electromagnetic waves and rough surfaces is typically performed either by analytical methods or by numerical simulations. In 1949, Morgan [2] used the finite-difference method to solve a quasi-static eddy-current problem for a 2-D periodic rough surface. He computed the ratio of the power loss dissipated in a conductor with a rough surface (P) to that dissipated in the same conductor with a smooth surface (P_0). This power loss ratio (P/P_0) is equal to the ratio of the attenuation constant due to conductor loses of a TEM transmission line with rough conductor surfaces (α_c) to that for the same line with smooth conductor surfaces (α_{c0}). Both rectangular and equilateral triangular roughness profiles were analyzed. The case of the current flowing transverse to the grooves is fully treated, while only a high-frequency asymptote for P/P_0 is given for the case of the current flowing parallel to the grooves. Two decades later, Sobol [3] applied Morgan's theory to microstrip lines and calculated P/P_0 for equilateral triangular grooves transverse to current flow as a function of the root-mean-square (rms) value for roughness. Sanderson [4] used the Rayleigh–Rice method to study the effect of periodic grooves transverse to the current flow on propagation of the TEM mode in a parallel-plate line.

Manuscript received September 19, 2006; revised November 10, 2006. This work was supported by the Defense Advanced Research Projects Agency–Microsystems Technology Office under the 3-D Micro-Electromagnetics Radio Frequency Systems (3d MERFS) Program.

The authors are with the Department of Electrical and Computer Engineering, University of Colorado at Boulder, Boulder, CO 80309-0425 USA (e-mail: milan.lukic@colorado.edu; dejan@colorado.edu).

Digital Object Identifier 10.1109/TMTT.2007.891688

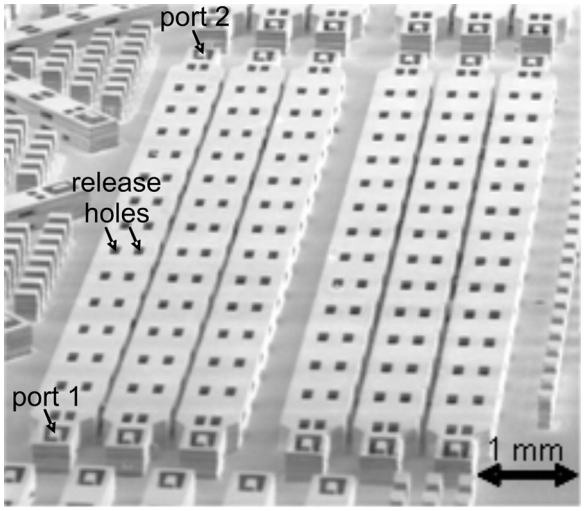

Fig. 1. Scanning electron microscope (SEM) photograph of several μ-coaxial lines built using the PolyStrata process [10].

The assumptions that need to be satisfied for the validity of this method are that the height of the surface roughness is small compared with a wavelength and that the height scale of the roughness is small compared with its width scale. Several authors have recently studied periodic [5], [6], as well as random [7] 2-D roughness profiles using different methods. Holloway and Kuester [5] calculated the power loss associated with 2-D periodic conducting and superconducting rough interfaces using a generalized impedance boundary condition, which they derived by applying the method of homogenization. Matsushima and Nakata [6] utilized the equivalent source method to numerically study periodic rectangular, triangular, and semielliptical grooves both transverse and parallel to current flow. In [7], the effects of random 2-D transverse surface roughness are analyzed by using two methods: the analytic small perturbation method and the numerical method of moments.

In this paper, effects of periodic 3-D surface roughness on a complex propagation constant (γ) of TEM transmission lines are studied using the commercial finite-element method (FEM) software High Frequency Structure Simulator (HFSS) [8] by solving for fields inside conductors [9]. The modeling approach is described, thoroughly validated, and used for the analysis of several 2-D and 3-D roughness profiles. It is also applied to calculate the excess loss due to the surface micromachined air-filled rectangular μ-coaxial lines [10]–[12], shown in Fig. 1.

This paper is organized as follows.

- Section II describes the proposed modeling approach and demonstrates its validity by comparison with analytical and

available literature results for the special case of 2-D surface roughness.

- Section III presents studies for the effects of several 2-D roughness profiles, specifically periodic rectangular, semicircular, and triangular grooves both transverse and parallel to current flow. A formula for equilateral triangular grooves transverse to current flow is derived and compared to the commonly used formulas.
- Section IV presents results for the effects of various 3-D roughness shapes, specifically periodic cubical, semiellipsoidal, and pyramidal indentations in conductor surfaces. The FEM results are compared with those obtained using finite-integration technique within the CST Microwave Studio [13].
- Section V gives a brief discussion of the effects of 3-D surface roughness on the phase constant.
- In Section VI, the developed model is applied to compute the excess loss due to the surface roughness of a micromachined recta-coax line. Measured data are also presented.
- Section VII summarizes the presented study.

II. Modeling

A. Modeling Approach

To evaluate the effects of an arbitrary 3-D surface roughness shape on amplitude and phase of the traveling TEM wave, we utilized inherent capabilities of the FEM implemented within the HFSS. Specifically, metal is modeled as a dielectric so that the mesh is created inside conductors with rough surfaces. Consequently, a natural boundary condition, which is the continuity of tangential components of the electric and magnetic field, is enforced at the rough interface between the conductor and dielectric. A short section of a transmission line with length l is simulated using the FEM, and its complex propagation constant γ is extracted from the S_{21}-parameter using the equation $S_{21} = e^{-\gamma l} = e^{-\alpha l}e^{-j\beta l}$. Herein, S_{21} is computed with respect to the characteristic impedance of the line obtained from the 2-D eigensolution of the line's cross section.

It is well known that high-frequency fields penetrate only into the shallow surface region of a thick good conductor. To reduce the size of the computational domain, the regions of the conductor where the fields are negligible are treated as perfect electric conductor. Thus, the mesh is generated and the fields are calculated only in the thin surface regions of the conductors. To determine their thickness, several TEM transmission lines with smooth conductor surfaces are modeled.

Fig. 2 shows simulated results for the attenuation constant α_c at 26 GHz as a function of normalized thickness of the meshed surface conductor region for a square coaxial line, circular coaxial line, and parallel-plate line. The separation between the conductors is 75 μm for all three lines. Also shown are analytical values for α_c for the circular coaxial and parallel plate lines of 0.167 and 0.149 dB/λ, respectively. The attenuation constant of 0.183 dB/λ for the square coax is obtained by the Schwartz–Christoffel conformal mapping in conjunction with Wheeler's incremental inductance rule [11]. The relative deviations of the simulated results with respect to the referenced results are also given. As seen, the conductor thickness of 1.5δ amounts to approximately 10% relative deviation. On the other hand, the results converge to 99.5%, and 99.9% of reference values when the conductor thickness is approximately 3δ and 5δ, respectively. In the subsequent simulations, we have used 5δ-thick meshed conductor regions underneath the grooves and indentations. Notice that the convergence history for all three analyzed TEM lines is almost the same. In this study, the size of the computational domain was greatly reduced by using symmetry. Specifically, 1/8th of a square coax, a small wedge-shaped part of a circular coax, and a very narrow section of a parallel-plate line are simulated. The size of the computational domain for the parallel-plate line is significantly smaller than for the other two lines, particularly much smaller than for the square coax. For this reason and since the convergence histories of the lines are virtually indistinguishable, the parallel-plate lines with rough conductor surfaces are studied in the following sections.

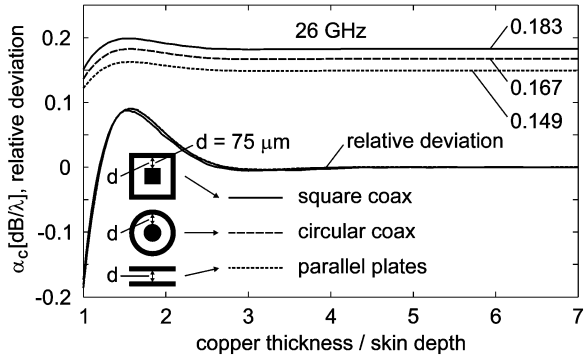

Fig. 2. Convergence of α_c versus normalized thickness of the meshed surface conductor region for square and circular coaxial lines and a parallel-plate line.

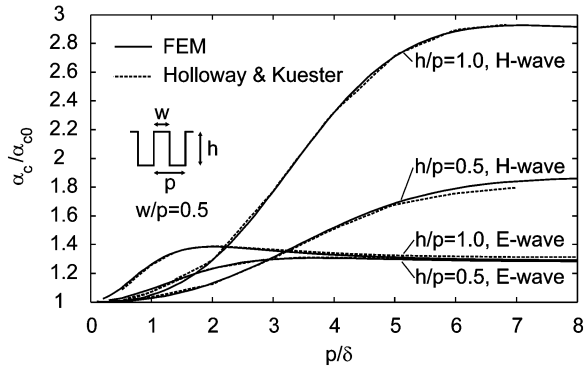

Fig. 3. Comparison between the literature [5] and our FEM-based modeling approach for rectangular grooves transverse (H-wave) and parallel to current flow (E-wave). Additional validation curves can be found in [9].

B. Validation

The modeling approach is validated using Holloway and Kuester's results [5] for rectangular grooves in conductor surfaces. The results for α_c/α_{c0} versus p/δ for the grooves transverse (H-wave) and parallel to current flow (E-wave) are shown in Fig. 3, and are in good agreement with the reference results. Note that Matsushima and Nakata [6] have also found their results to be in good agreement with those in [5]. For the case of grooves transverse to current flow, it is observed

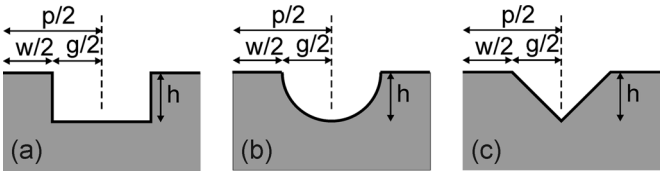

Fig. 4. One period of 2-D surface roughness profiles. (a) Rectangular. (b) Semicircular. (c) Triangular. The profiles are symmetric with respect to the dashed line.

that the ratio α_c/α_{c0} approaches an asymptotic value as p/δ gets very large, i.e., at very high frequencies. Low-frequency currents flow below the grooves, thus the roughness effects are insignificant. However, at high frequencies, the current and fields in the conductor are forced near the surface, and a larger fraction of the total current is affected by the roughness [5]. The interested reader is referred to [6, Fig. 3], which shows contour lines of field intensity inside a conductor for grooves transverse and parallel to current flow. For transverse grooves, the high-frequency currents are forced to follow the path of the roughness profile, thus an estimate for the α_c/α_{c0} asymptote can be calculated as the ratio of the path length on the rough surface to that of the smooth surface. For example, for the two H-wave curves in Fig. 3, the estimated asymptotes, computed as $1+2h/p$, are 2 and 3.

III. 2-D Roughness

A. 2-D Profiles

The modeling approach explained in Section II is applied here to study several 2-D surface roughness profiles. Fig. 4 shows one period of the profiles with geometrical parameters (p, w, g, and h) for rectangular, semicircular, and triangular grooves. For any roughness profile, the rms value for roughness (Δ) can be expressed in terms of its dimensional parameters. For example, $\Delta = p/4$ for an equilateral triangular profile with $w = 0$, and $\Delta = h/p\sqrt{w(p-w)}$ for a rectangular profile. A detailed description of calculations of Δ can be found in [2]. The results for the grooves transverse and parallel to current flow are presented in Sections III-B and C.

B. Grooves Transverse to Current Flow

Increased conductor losses due to surface roughness are usually computed by [14]

$$\frac{\alpha_c}{\alpha_{c0}} = 1 + \frac{2}{\pi}\tan^{-1}\left(1.4\left(\frac{\Delta}{\delta}\right)^2\right) \tag{1}$$

where Δ/δ is the normalized rms roughness. This formula was obtained by curve-fitting measured data sets obtained with microstrip lines. It also agrees very well with the theoretical predictions in [3], derived for the equilateral triangular grooves transverse to the current flow. Expression (1) is often implemented for other transmission lines and roughness shapes. For example, in [15], it is used for a micromachined recta-coax, while its validity for any transmission line is argued in [16]. Roughness effects on the line losses are also computed by [17]

$$\frac{\alpha_c}{\alpha_{c0}} = 1 + \exp\left(-\left(\frac{\delta}{2\Delta}\right)^{1.6}\right) \tag{2}$$

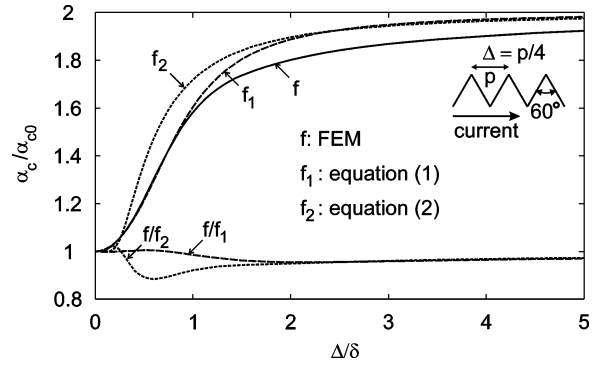

Fig. 5. Relative change of the attenuation constant α_c versus normalized rms value for roughness for equilateral triangular grooves transverse to current flow. The solid line, denoted by f, represents the FEM results obtained with our modeling approach.

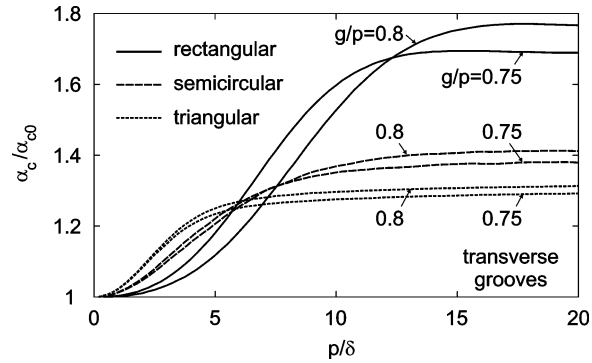

Fig. 6. Relative change of the attenuation constant α_c versus normalized roughness period for rectangular, semicircular, and triangular grooves in conductor surfaces transverse to current flow: $h = g/2$.

obtained from the measurements of the quality factor of the cavity resonators.

By applying the modeling approach from Section II on the same roughness profiles for which (1) is derived, somewhat different results are obtained. Specifically, (3) fits the computed results, shown in Fig. 5, to within 1.5% as follows:

$$\frac{\alpha_c}{\alpha_{c0}} = 1 + \frac{2}{\pi}\tan^{-1}\left(\left(\frac{\Delta}{\delta}\right)^2\left(0.094\left(\frac{\Delta}{\delta}\right)^2 - 0.74\left(\frac{\Delta}{\delta}\right) + 1.87\right)\right). \tag{3}$$

Expressions for α_c/α_{c0} given by (1) and (2) are also plotted in Fig. 5. As seen, our results agree with (1) to within 1.6% for Δ smaller than one skin depth, and within 4.5% for larger Δ's. Although somewhat more complicated than (1) and (2), the derived formula (3) can be easily implemented in any software formulated to account for a finite conductivity of the metals. Note that all three formulas have the small skin depth limit of 2 equal to the ratio of the path length on the rough surface to that of the smooth surface.

Fig. 6 shows simulation results for α_c/α_{c0} as a function of normalized roughness period for transverse rectangular, semicircular, and triangular grooves of Fig. 4 with $h = g/2$. For $g/p = 0.8$, the high-frequency asymptotes for α_c/α_{c0} calculated as the ratio of the path lengths for rectangular, semicircular, and triangular profiles are approximately 1.8, 1.46, and 1.33, respectively. For $g/p = 0.75$, these asymptotes are approximately

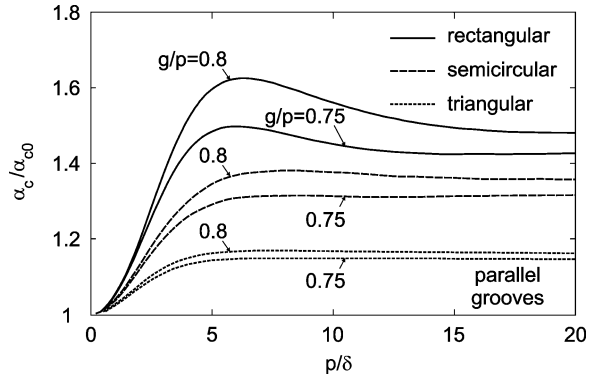

Fig. 7. Relative change of the attenuation constant α_c versus normalized roughness period for rectangular, semicircular, and triangular grooves in conductor surfaces parallel to current flow: $h = g/2$.

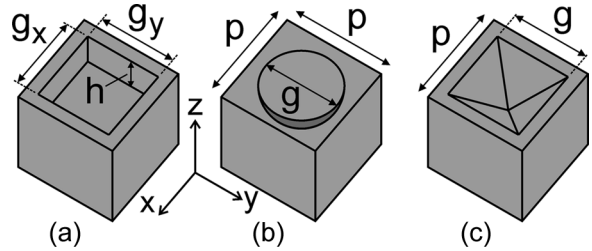

Fig. 8. Unit cells of periodic: (a) cubical, (b) semiellipsoidal, and (c) pyramidal indentations in a conductor surface. The depth for all three shapes is denoted by h and, for clarity, it is shown only for cubical indentations.

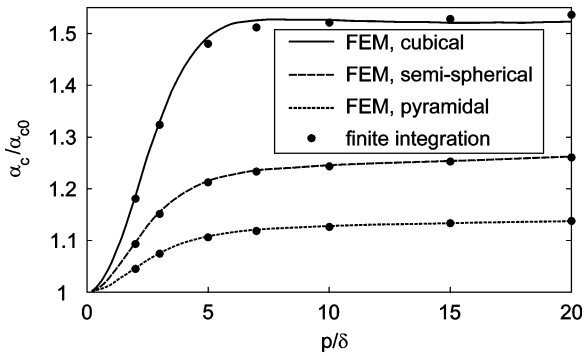

Fig. 9. Comparison between the FEM and finite-integration technique results for relative change of the attenuation constant α_c for cubical, semispherical, and pyramidal indentations in conductor surfaces: $g/p = 0.75$, $h = g/2$.

1.75, 1.43, and 1.31. Notice that in these studies, the normalized parameters h/p and g/p are varied simultaneously since $h = g/2$, and that the parameter $w/p = 1 - g/p$ is equal to 0.25 and 0.2 for g/p equal to 0.75 and 0.8, respectively. The effect of the parameter w/p on α_c/α_{c0} for transverse rectangular grooves for a constant value of $h/p = 0.5$ is given in [5, Fig. 7]. We have obtained the same results; however, here we only provide some relevant observations. First, the high-frequency asymptote for α_c/α_{c0} for this case is $1 + 2h/p$, as explained above, and thus, it does not depend on w/p. However, at low frequencies, the ratio α_c/α_{c0} is much larger for larger values of w/p. This could be intuitively expected because wider metallic walls, of width w, forming the transverse grooves, represent a larger obstacle for the current flowing underneath them. Namely, the current gets more diverted into wider walls traveling longer paths, and thus, creating more additional loss. It can be seen that, in Fig. 6, the curves for g/p equal to 0.75 and 0.8 intersect for rectangular and semicircular grooves. Specifically, α_c/α_{c0} has smaller values for larger values of g/p corresponding to much smaller values of w/p and slightly larger h/p. For rectangular grooves, this can be expected based on the above observations. Namely, the slightly larger h/p causes an increase in α_c/α_{c0}, as seen in Fig. 3, but the decrease of α_c/α_{c0} due to much smaller w/p is more dominant. It is interesting that a similar behavior is observed for semicircular grooves, but not for triangular grooves. It is also observed that α_c/α_{c0} at high frequencies is largest for rectangular and smallest for triangular grooves, while the situation is exactly the opposite at low frequencies.

C. Grooves Parallel to Current Flow

Simulation results for α_c/α_{c0} as a function of the normalized roughness period for parallel rectangular, semicircular, and triangular grooves of Fig. 4 are shown in Fig. 7 for g/p equal to 0.75 and 0.8, i.e., w/p equal to 0.25 and 0.2. As for the transverse grooves, low-frequency current flows beneath the grooves and only a small percent of the total current "sees" the roughness, resulting in a small additional power loss above that of a smooth conductor [5]. However, as the frequency increases, the current gets more diverted into the metallic walls, of width w, forming the parallel grooves. A drawing of contour lines of field intensity inside a conductor that illustrates this can be found in [6, Fig. 3(b) and (d)]. The effect of the parameter w/p on α_c/α_{c0} for parallel rectangular grooves for a constant value of $h/p = 0.5$ is given in [5, Fig. 10], which we have also demonstrated in [9, Fig. (2b)]. An important observation from that study was that narrower walls cause larger α_c/α_{c0} at all frequencies. This could be intuitively expected, especially at very high frequencies at which the current emerges to the uppermost part of roughness walls while the conductor surface right underneath the grooves gets depleted of current. It is then also expected that the effect on α_c/α_{c0} is largest for rectangular and smallest for triangular grooves, as seen in Fig. 7. This is so because the width of the walls for triangular grooves increases linearly from w to p as the depth increases from 0 to h, while for rectangular grooves it remains constant.

IV. 3-D Roughness

The effect of periodic cubical, semiellipsoidal, and pyramidal indentations in the conductor surface on the line attenuation constant is studied here.

A. 3-D Profiles

The geometrical parameters of studied 3-D roughness shapes, as well as the reference coordinate system, are shown in Fig. 8. The indentations are periodic in the x- and y-direction with periodicity p. Their depth is denoted by h for all three shapes, though this dimension is only depicted in Fig. 8(a) for clarity.

An excellent agreement between the FEM and finite-integration technique results is demonstrated in Fig. 9. It is noticed that for the same values of the roughness period p and the parameters g and h, the effect on α_c/α_{c0} is largest for cubical and smallest for pyramidal indentations.

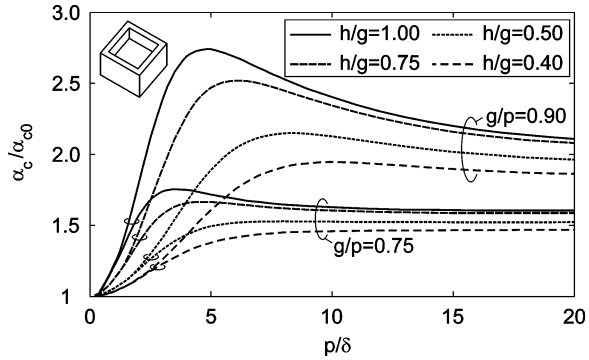

Fig. 10. Relative change of the attenuation constant α_c for cubical indentations in conductor surfaces: $g_x = g_y = g$.

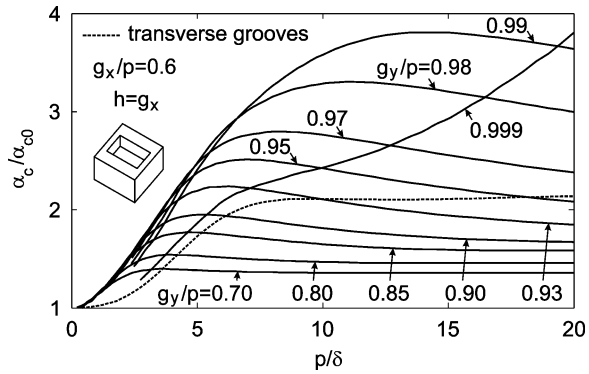

Fig. 11. Relative change of the attenuation constant α_c for cubical indentations with varying width g_y and $g_x = h$.

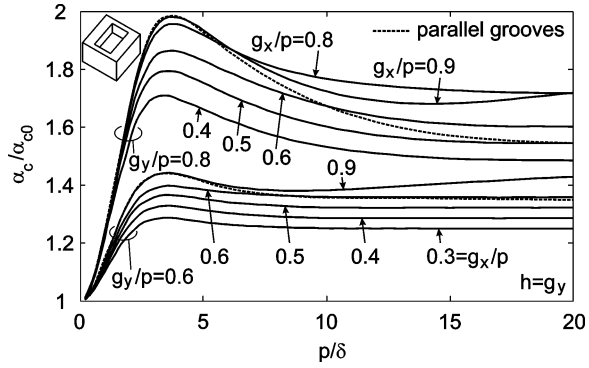

Fig. 12. Relative change of the attenuation constant α_c for cubical indentations with varying length g_x for two values of g_y and $h = g_y$.

B. Cubical Indentations

The results for cubical indentations are plotted in Figs. 10–12. In the study presented in Fig. 10, the base of the cube is square ($g_x = g_y = g$) and two values of filling factor g/p, i.e., 0.75 and 0.9, are considered. Four heights, i.e., $h/g = 0.4, 0.5, 0.75$, and 1, are taken for each g/p value. If the current flows in the x-direction in Fig. 8, then the metallic walls parallel to the y–z-plane represent the obstacle like the walls of transverse grooves studied above, and the walls parallel to the x–z-plane are like those of parallel grooves. It is then expected that the relative change of the attenuation constant is larger for larger values of the normalized dimension h/g, as seen in Fig. 10. It is also observed that the small skin-depth asymptote for α_c/α_{c0} is predominantly determined by the value of $g/p = 1 - w/p$ and less by h/g. On the contrary, for large skin depths, i.e., at lower frequencies, α_c/α_{c0} is primarily dependent on h/g and is virtually independent on g/p. Note that the widths of walls parallel to the x–z- and y–z-plane are equal and varied simultaneously. According to the above discussed studies of the effects of the transverse and parallel wall widths on α_c/α_{c0} at low frequencies, an increase of w/p results in the increase of the contribution to α_c/α_{c0} in the transverse walls and its decrease in the parallel walls. The two effects compensate and, as a result, α_c/α_{c0} is almost independent of g/p at low frequencies. However, at high frequencies, the parameter w/p is not so important for transverse grooves as it is for parallel grooves and α_c/α_{c0} is larger for larger g/p, as seen in Fig. 10.

The effects of varying either width g_y or length g_x of the cubical indentations when the other dimensions are fixed are demonstrated in the next two studies. The E- and H-field are polarized in the z- and y-direction, respectively, thus the TEM wave propagates in the negative x-direction. The results for α_c/α_{c0} for varying g_y (fixed g_x and $h = g_x$) and varying g_x (fixed g_y and $h = g_y$) cases are shown in Figs. 11 and 12, respectively. Notice that, for the former case, the indentations merge into rectangular grooves transverse to the current flow when $g_y/p = 1$. Similarly, for the later case, the indentations merge into rectangular grooves parallel to the current flow when $g_x/p = 1$. Dashed lines in Figs. 11 and 12 are the results for corresponding 2-D roughness profiles.

As seen in Fig. 11, for $g_y/p \leq 0.95$, α_c/α_{c0} is virtually unaffected by g_y/p for small p/δ. Note that the high-frequency asymptote of 2.2, which is calculated as $1 + 2h/p$, is estimated for α_c/α_{c0} for transverse grooves of normalized height $h/p = 0.6$. Eventually, for g_y/p very close to unity (see curve for $g_y/p = 0.999$), the results for α_c/α_{c0} start to approach these for the corresponding transverse grooves. Notice that, at low frequencies, when $p/\delta < 2$, α_c/α_{c0} for transverse grooves is significantly lower than for cubical indentations for g_y/p less than 0.95. Only for g_y/p very close to unity do low-frequency values of α_c/α_{c0} for cubical indentations become as small as for corresponding transverse grooves. For g_y/p very close to unity, the cubical indentations are almost merged into rectangular grooves, except for thin metallic membranes of thickness $p - g_y$ periodically located across the grooves. The above results then imply that the effect of such thin membranes on α_c/α_{c0} is very significant at all frequencies.

The results of a varying g_x case are given in Fig. 12 for g_y/p of 0.6 and 0.8. It is observed that the convergence toward the results for the corresponding 2-D roughness profile is much faster than for the above case of varying g_y. This implies that, for this orientation of the grooves, the effect of the thin metallic membranes periodically located across the grooves is small, especially at low frequencies.

C. Semiellipsoidal and Pyramidal Indentations

Effects of the height of semiellipsoidal and pyramidal indentations on α_c/α_{c0} for 100% filling factor ($g/p = 1$) are shown in Figs. 13 and 14, respectively. It is observed that for the same height, α_c/α_{c0} is much higher for the former case. Roughly,

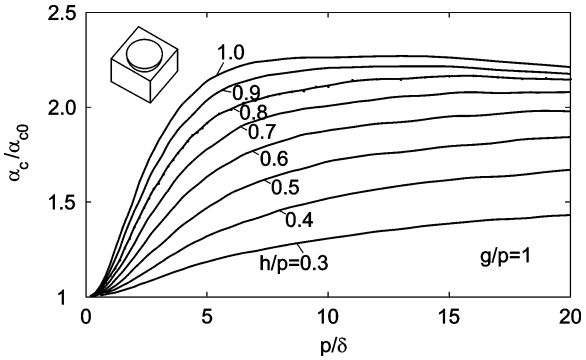

Fig. 13. Relative change of the attenuation constant α_c for semiellipsoidal indentations in conductor surfaces for different heights of indentations.

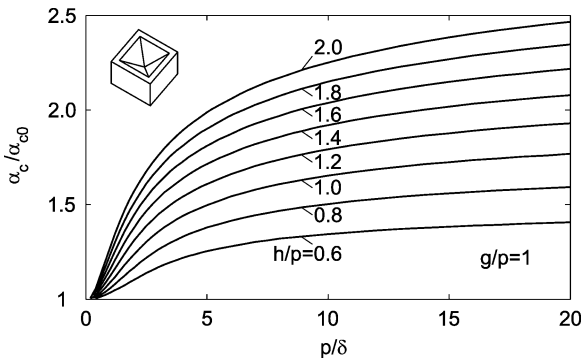

Fig. 14. Relative change of the attenuation constant α_c for pyramidal indentations in conductor surfaces for different heights of indentations.

about a twice-larger height is needed for pyramidal indentations for about the same value of α_c/α_{c0}. It is observed that the simulated α_c/α_{c0} curves for the semiellipsoidal indentations were not as smooth as for other results here. This is attributed to the small geometrical errors occurring because tetrahedras are used in meshing of elliptical curvatures. Smoother α_c/α_{c0} curves can be obtained if special care is taken in creating the mesh. Actual simulation results for the case $h/p = 0.8$ are shown via dots in Fig. 13 and are replaced with the solid line denoted by 0.8, likewise for the other h/p cases.

D. Discussion

Results presented here clearly demonstrate that the 3-D roughness can be accurately modeled with either the FEM or finite-integration technique. It is also shown that the level of increase in conductor losses is dependent on the shape and distribution of indentations. The simulations here have typically used approximately 3 GB of random access memory. It took on average 1 h of running time on a 2.8-GHz Intel Pentium D processor for each of the curves in Figs. 9–14. The memory requirements for longer lines with realistic 3-D rough profiles impose severe modeling restrictions. Nevertheless, the studies and plots presented here can be used very effectively in estimating the additional losses due to the similar imperfections in the conductor surfaces.

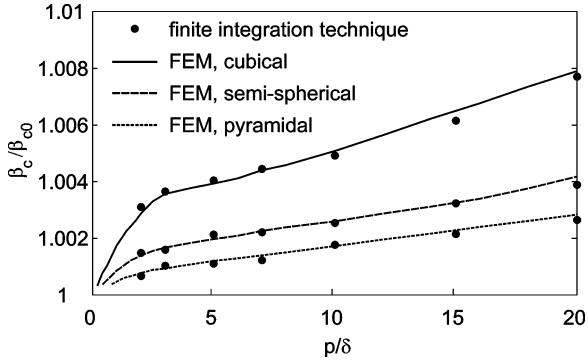

Fig. 15. Comparison between the FEM and finite-integration technique results for the relative change of the phase constant β_c for cubical, semispherical, and pyramidal indentations in conductor surfaces: $g/p = 0.75$, $h = g/2$.

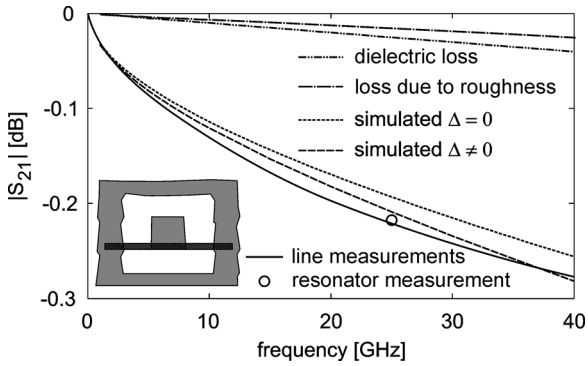

Fig. 16. Comparison between the measured and simulated $|S_{21}|$ for a 1-cm-long recta-coax line. Δ denotes the rms value for roughness of the recta-coax conductor surfaces, as shown in Fig. 17. The circle represents the line loss at 25 GHz extracted from a half-wavelength transmission line resonator measurement.

V. Phase Constant

Simulation results for the ratio of the phase constant of the line with rough conductor surfaces (β_c) to that for the same line with smooth conductor surfaces (β_{c0}) as a function of the normalized period for cubical, semispherical, and pyramidal indentations are shown in Fig. 15. Note that, for this study, the separation between the conductors of a parallel-plate line was 50 μm. As seen, FEM and finite-integration technique results agree very well. It is also noticed that the effect on β_c/β_{c0} is largest for cubical and smallest for pyramidal indentations. Presented results show the small effect roughness will have on the line electrical length, nevertheless the utility of the modeling approach for determining this parameter (if needed) is clearly demonstrated.

VI. Measurements

Here, the developed roughness model is used to compute the excess loss of μ-rectangular coaxial lines shown in Fig. 1. The measured result for the averaged insertion loss of several recta-coax lines is given in Fig. 16 along with relevant simulations. The measurement setup includes an HP-8510C network analyzer with Cascade Microtech 150-μm-pitch coplanar waveguide (CPW) microwave probes and a Cascade Summit 9000 probe station. An external short-open-load-thru calibration implementing CPW on an alumina substrate is used for the two-port calibration. Effects of the launch sections, whose design can be found in [18], are deembedded using the results

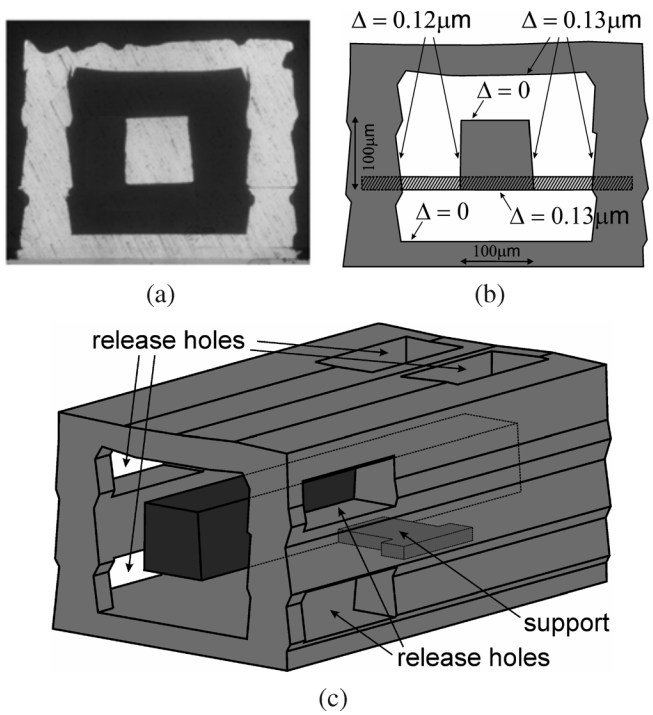

Fig. 17. (a) Cross section of realized recta-coax line. (b) Cross section of the line as simulated by FEM with values for rms roughness for individual conductor surfaces. (c) 3-D view of the simulated section of the recta-coax.

from the back-to-back launches. Also given in Fig. 16 is the line loss at 25 GHz, as extracted from the μ-coaxial transmission line resonator measurements.

Shown in Fig. 17(a)–(c) is a photograph of a cross section of the fabricated line, the cross section of the line with periodic dielectric supports for the inner conductor as modeled with FEM, and a 3-D view of the simulated section of the recta-coax. Inner and outer conductor sizes are 100×100 μm^2 and 250×250 μm^2, respectively. Dielectric supports embedded in the sidewalls are 18-μm thick and 100-μm wide. They span the distance of 250 μm between the sidewalls of the line and are periodically placed along the line with periodicity of 700 μm. Their dielectric constant and $\tan\delta$ are 2.85 and 0.045, respectively. The release holes are needed to enable the removal of sacrificial photoresist, and their designed dimensions in the sidewalls and top walls are 75×200 and 100×200 μm^2, respectively.

The line from Fig. 17 is first simulated assuming that all conductor surfaces are perfectly smooth. This is denoted by $\Delta = 0$ in Fig. 16. Note that Schwartz–Christoffel conformal mapping in conjunction with Wheeler's incremental inductance rule [11] can alternatively be used for calculation of the losses for the line with smooth conductors. However, the incremental inductance rule cannot be used to estimate the additional losses due to surface roughness. These losses are taken into account, via FEM, in the second simulation of Fig. 16, and the obtained curve for the magnitude of the S_{21}-parameter is denoted by $\Delta \neq 0$. The loss contribution due to roughness is also plotted and, as expected, it monotonically increases with frequency, rising to 9.2% of the total loss at 40 GHz. Since the bandwidth for a single TEM mode operation of this recta-coax is approximately 467 GHz [11], the roughness effects would become more pronounced at frequencies beyond the measured frequency range.

TABLE I
VALUES OF $\kappa = \sigma/\sigma_c$ FOR INDIVIDUAL CONDUCTOR SURFACES OF THE RECTA-COAX LINE SHOWN IN FIG. 17, AND CONTRIBUTION OF THE SURFACE ROUGHNESS LOSSES AND DIELECTRIC LOSSES TO THE TOTAL LINE LOSS

frequency [GHz]		10	20	30	40
κ	Δ=0.12μm	1.074	1.146	1.216	1.285
	Δ=0.13μm	1.087	1.171	1.252	1.332
roughness loss [%]		5.7	6.9	8.1	9.2
dielectric loss [%]		8.4	11.1	12.9	14.3

In the above simulation, the bottom side of the outer conductor and the top side of the inner conductor are perfectly smooth. These conditions arise from the ability of the fabrication process to polish these horizontal copper surfaces to the optically fine smoothness. RMS roughness values of the remaining conductor surfaces shown in Fig. 17(b), as provided by the Mayo Foundation, are used in the following way. Owing to the inherent features of the FEM, the effects of surface roughness are modeled through a modified conductivity of the individual conductor surfaces. Specifically, the conductivity of a particular rough copper wall is $\sigma_c = \sigma/\kappa$, where $\sigma = 5.8 \cdot 10^7$ S/m is the bulk conductivity of the smooth conductor. The parameter $\kappa = (\alpha_c/\alpha_{c0})^2 \geq 1$ is determined from the measured rms roughness values and (3) obtained by the presented method. Its values for several frequencies within the measured frequency range are given in Table I. The skin depth δ at 40 GHz is approximately 0.33 μm; hence, $\Delta/\delta < 0.4$ below this frequency. Since (3) and (1) agree within 1.6% for these values of Δ/δ, (1) would give very similar values for the parameter κ. Also shown in Table I are the fractions of the total loss due to the roughness and dielectric loss. The effect of the release holes is also studied and it is found that their loss contribution is marginal.

These results show that, up to 40 GHz, the impact of the roughness on the overall losses of μ-coaxial lines is below 10%. However, these effects should be taken into account at higher frequencies when an accurate determination of the line losses is needed. Note that the direct solving for the fields inside the rough conductors for the realistic recta-coax line, shown in Fig. 17, is impractical. This is due to the lack of symmetries and associated excessive memory requirements needed to accurately mesh the interior of the metal walls. However, as demonstrated here, the roughness effects determined based on the simulations of a small section of a parallel-plate line, by the method described in Section II, can be readily applied.

VII. CONCLUSION

In this paper, the FEM has been used to calculate the effect of 3-D surface roughness on a propagation constant of TEM transmission lines. The surface region of conductors has been modeled as a dielectric so that the mesh is created inside the conductor volume of a rough profile. Consequently, a natural boundary condition enforced at the rough interface between the conductor and dielectric has insured its proper modeling. Modeling has been validated by comparison with available literature results for the special case of 2-D surface roughness profiles

and by simulations of 3-D roughness shapes using the finite-integration technique. The results for periodic cubical, semiellipsoidal, and pyramidal indentations, as well as rectangular, semicircular, and triangular grooves in conductor surfaces have been presented. The developed roughness model has been applied to compute excess losses of the surface micromachined rectangular μ-coaxial line.

ACKNOWLEDGMENT

The authors would like to thank Prof. Z. Popović, Prof. E. Kuester, Dr. S. Rondineau, and K. Vanhille, all with the University of Colorado at Boulder, G. Potvin and D. Fontaine, both with BAE Systems, Nashua, NH, Dr. C. Nichols and Dr. D. Sherrer, both with the Rohm and Haas Company, Blacksburg, VA, Dr. W. Wilkins and Dr. V. Sokolov, both with the Mayo Foundation, Rochester, MN, Dr. J. Evans, Defense Advanced Research Projects Agency–Microsystems Technology Office (DARPA–MTO), Arlington, VA, and E. Adler, Army Research Laboratory (ARL), Adelphi, MD, for useful discussions and support. The authors are also thankful to B. Brim, Ansoft Corporation, Boulder, CO, for many useful discussions.

REFERENCES

[1] K. F. Warnick and W. C. Chew, "Numerical simulation methods for rough surface scattering," *Waves Random Media*, vol. 11, pp. R1–R30, 2001.

[2] S. P. Morgan, "Effect of surface roughness on eddy current losses at microwave frequencies," *J. Appl. Phys.*, vol. 20, pp. 352–362, 1949.

[3] H. Sobol, "Application of integrated circuit technology to microwave frequencies," *Proc. IEEE*, vol. 59, no. 8, pp. 1200–1211, Aug. 1971.

[4] A. E. Sanderson, "Effect of surface roughness on propagation of the TEM mode," in *Advances in Microwaves*. New York: Academic, 1971, vol. 7, pp. 1–57.

[5] C. L. Holloway and E. F. Kuester, "Power loss associated with conducting and superconducting rough interfaces," *IEEE Trans. Microw. Theory Tech.*, vol. 48, no. 10, pp. 1601–1610, Oct. 2000.

[6] A. Matsushima and K. Nakata, "Power loss and local surface impedance associated with conducting rough interfaces," *Elect. Commun. Jpn.*, vol. 89, no. 1, pt. 2, pp. 1–10, Jan. 2006.

[7] L. Tsang, X. Gu, and H. Braunisch, "Effects of random rough surface on absorption by conductors at microwave frequencies," *IEEE Microw. Wireless Compon. Lett.*, vol. 16, no. 4, pp. 221–223, Apr. 2006.

[8] *"HFSS v10.0 User Manual,"* Ansoft Corporation, Pittsburgh, PA, 2005.

[9] M. Lukic and D. S. Filipovic, "Modeling of surface roughness effects on the performance of rectangular μ-coaxial lines," in *22nd Annu. Progr. Electromagn.*, Miami, FL, Mar. 2006, pp. 620–625.

[10] D. W. Sherrer and J. J. Fisher, "Coaxial waveguide microstructures and methods of formation thereof," U.S. Patent Applicat. US 2004/026390A1, Dec. 30, 2004.

[11] M. Lukic, S. Rondineau, Z. Popović, and D. S. Filipovic, "Modeling of realistic rectangular μ-coaxial lines," *IEEE Trans. Microw. Theory Tech.*, vol. 54, no. 5, pp. 2068–2076, May 2006.

[12] D. S. Filipovic, Z. Popović, K. Vanhille, M. Lukic, S. Rondineau, M. Buck, G. Potvin, D. Fontaine, C. Nichols, D. Sherrer, S. Zhou, W. Houck, D. Fleming, E. Daniel, W. Wilkins, V. Sokolov, and J. Evans, "Modeling, design, fabrication, and performance of rectangular μ-coaxial lines and components," in *IEEE MTT-S Int. Microw. Symp. Dig.*, San Francisco, CA, Jun. 2006, pp. 1393–1396.

[13] *"CST Microwave Studio User Manual, Version 2006.0.0,"* CST GmbH, Darmstadt, Germany, 2006.

[14] E. Hammerstad and O. Jensen, "Accurate models for microstrip computer-aided design," in *IEEE MTT-S Int. Microw. Symp. Dig.*, Washington, DC, May 1980, pp. 407–409.

[15] J. R. Reid, E. D. Marsh, and R. T. Webster, "Micromachined rectangular-coaxial transmission lines," *IEEE Trans. Microw. Theory Tech.*, vol. 54, no. 8, pp. 3433–3442, Aug. 2006.

[16] D. M. Pozar, "Transmission line theory," in *Microwave Engineering*. Hoboken, NJ: Wiley, 2005, ch. 2, p. 86.

[17] S. Groiss, I. Bardi, O. Biro, K. Preis, and K. Richter, "Parameters of lossy cavity resonators calculated by the finite element method," *IEEE Trans. Magn.*, vol. 32, no. 3, pp. 894–897, May 1996.

[18] K. J. Vanhille, D. L. Fontaine, C. Nichols, D. S. Filipovic, and Z. Popović, "Quasi-planar high-Q millimeter-wave resonators," *IEEE Trans. Microw. Theory Tech.*, vol. 54, no. 6, pp. 2439–2446, Jun. 2006.

Milan V. Lukić (S'02) received the Dipl. Eng. degree in electrical engineering from the University of Banjaluka, Banjaluka, Bosnia and Herzegovina, in 1998, the M.S.E.E. degree from the University of Mississippi, University, in 2002, and is currently working toward the Ph.D. degree at the University of Colorado at Boulder.

His research interests include multilayered rectangular waveguide dyadic Green's functions, mode matching, conformal mapping (CM), transmission lines, and antennas.

Mr. Lukić was the recipient of the 2002 Graduate Achievement Award presented by the University of Mississippi, and the 1998 Gold Medal presented by the University of Banjaluka.

Dejan S. Filipovic (S'99–M'02) received the Dipl. Eng. degree in electrical engineering from the University of Nis, Nis, Serbia, in 1994, and the M.S.E.E. and Ph.D. degrees from The University of Michigan at Ann Arbor, in 1999 and 2002, respectively.

From 1994 to 1997, he was a Research Assistant with the University of Nis. From 1997 to 2002, he was a graduate student with The University of Michigan at Ann Arbor. He is currently an Assistant Professor with the University of Colorado at Boulder. His research interests are in the development of millimeter-wave components and systems, multiphysics modeling, antenna theory and design, as well as in computational and applied electromagnetics.